IEEE Access
Multidisciplinary ⋮ Rapid Review ⋮ Open Access Journal

Received 20 May 2022, accepted 30 May 2022, date of publication 2 June 2022, date of current version 29 June 2022.

Digital Object Identifier 10.1109/ACCESS.2022.3179818

Data-Driven Modeling and Prediction Analysis for Surface Roughness of Special-Shaped Stone by Robotic Grinding

FANGCHEN YIN, QINGZHI JI, AND CHANGCAI CUN

National and Local Joint Engineering Research Center for Intelligent Manufacturing Technology of Brittle Material Products, Huaqiao University, Xiamen 361021, China
Institute of Manufacturing Engineering, Huaqiao University, Xiamen 361021, China

Corresponding author: Changcai Cun (cuichc@hqu.edu.cn)

This work was supported in part by the National Natural Science Foundation of China under Grant U1805251 and Grant 51905181 and in part by the Natural Science Foundation of Fujian Province under Grant 2019J01084. The work of Fangchen Yin was supported by the Fundamental Research Funds for the Central Universities under Grant ZQN-801.

ABSTRACT This paper aims to accurately predict the surface quality of the special-shaped stone by robotic grinding and effectively guide the adjustment of process parameters to ensure stable grinding quality, applies a support vector machine model based on improved whale optimization algorithm (IWOA-SVR), so as to establish a prediction model of surface roughness of special-shaped stone and a selection method of process parameters. The proposed IWOA-SVR was used to improve the prediction accuracy of support vector machine regression model, and a prediction model of surface roughness (R_a) for stone was established. On this basis, the relationship between the output parameters (surface roughness) and inutput parameters (spindle speed, feed speed, cutting depth and cutting width)was explored to obtain more suitable process parameters. Combining the grinding experiment data of special-shaped stone, the comparison was carried out between IWOA-SVR and the SVR model optimized by the commonly used optimization algorithms (grid-search optimization algorithm (GS) and whale optimization algorithm (WOA)). Under the same sample condition, the prediction error of GS-SVR is the most large, and the average prediction error of IWOA-SVR is only 86.1% if that of WOA-SVR, the training time is shortened by 54.4%. The influence of process parameters on surface roughness obtained by IWOA-SVR can effectively guide the selection and adjustment of process parameters. It has good guiding significance for maintaining the excellent grinding quality of special-shaped stone.

INDEX TERMS Special-shaped natural stone, grinding complexity, surface roughness.

I. INTRODUCTION

The application of robotic manipulators for the SNS products can make up for the shortcomings of traditional numerical control machining, such as the small working range, the inability to machine large and extremely large sculptures, and poor machining posture [1]. Additionally, diamond grinding tools have been widely used in the field of stone grinding because of their long tool life and strong wear resistance [2]. However, due to the weak stiffness structure of the robotic manipulators and the hard brittleness and complex structure characteristics of SNS, the natural stone blank is easy to collapse or fracture, so the selection of grinding process parameters is put forward higher requirements with the accurate prediction of the trend of processing quality, so as to effectively guide the selection and adjustment of process parameters to ensure the stability of processing quality of SNS products, which is an effective and low-cost way to promote the large-scale application of mechanical arm in the field of stone grinding [3], [4]. Surface roughness is the most effective index to measure the quality of stone processing. Meanwhile, the measurement of surface roughness of stone is a very time-consuming process. It should be pointed out that surface roughness prediction model with high precision is not only the basis of controlling and stabilizing surface roughness but also can avoid the high-cost and long-time measurement process. Over the past decades, many researchers have been carried out for establishing surface roughness prediction

The associate editor coordinating the review of this manuscript and approving it for publication was Mohammad Alshabi.

model of machining process, which can be approximately fall into three categories: theoretical method [5], experimental design method [6], and artificial intelligence (AI) method [7].

In the first category, according to the generative grinding principle of face gears and the mathematical model of tooth surface, Wang *et al.* (2017) analyzed the formation mechanism of surface roughness when the disk wheel is generated into grinding face gears and established the calculation model of surface roughness for the generative grinding along the contact line of face gear tooth surface [8]. Dai *et al.* (2021) established the surface roughness model of hard and brittle materials in axial ultrasonic vibration grinding considering the influence of overlapping effect of abrasive particle motion trajectory [9]. For diamond wire saw machining, Li *et al.* (2020) used truncated Gaussian distribution model to represent the wear of wire saw and provided a theoretical model of surface roughness according to the relative motion of wire saw and workpiece [10]. Shen (2006) established a surface roughness prediction model for ultra-precision machining microlens array in regarded with the relative influence of the 3D direction between the tool and the workpiece [11]. To sum up, the modeling method of theoretical analysis is widely used because it can deeply analyze the formation mechanism of surface roughness, but its modeling accuracy is closely related to the parameters of the material constitutive model, resulting in complicated and difficult practical application.

In the second category, the surface roughness model is established in various machining by experimental design method. Ma *et al.* (2014) made theoretical analysis on the influencing factors of surface roughness in form grinding and studied the relationship between grinding parameters and grinding surface roughness by designing full-factor experiments [12]. Wang *et al.* (2015) studied the influence of grinding process parameters on the surface roughness of formed grinding teeth by response surface methodology, carried out multiple regression analysis on the experimental results and established a prediction model of surface roughness [13]. In addition, Majumder *et al.* (2018) took the rotary copper-tungsten alloy specimen in low-speed wire-cut EDM as the research object and analyzed the influence law of different speed parameters on the surface roughness of the workpiece and the optimal combination of process parameters by using the response surface method [14]. The response surface method has the advantages of strong generalization ability and high prediction accuracy. It can not only use multiple quadratic regression equation to describe the functional relationship between independent variables and roughness, but also reflect the interaction between variables. However, this modeling method requires more test data and the cost of formula is high [15].

In addition to the above two methods, AI method with its strong feature mapping ability and nonlinear fitting ability has also been widely used in the prediction of surface roughness in molding [16]. Currently, the most widely used method of AI method in the prediction of surface roughness is artificial neural network algorithm [17]. For example, Ahilan et al designed a BP neural network based turning surface roughness prediction model in which different process parameters are taken as input features. The results indicates that the neural network model has better prediction results compared with the experimental measured values of turning ordinary steel [18]. Karkalos *et al.* (2016) used the cyclic algorithm to compare the optimal number of neurons in the hidden layer, and established a grinding surface roughness prediction model based on the RBF neural network, which was verified by experiments on a high-speed cylindrical grinder [19]. It should be pointed out that the neural network method has some inherent defects such as difficulties of determining the network structure, over-learning, slow convergence rate, poor generalization ability and local extremums [20]. Support vector machine (SVM) is a kind of supervised machine learning methods based on structural risk minimization criterion to construct, it can reduce model for fitting the probability, and is not sensitive area of the structure can absorb in the random response of small random fluctuations compared to minimize guidelines based on experience to build artificial neural network [21]. Therefore, it is widely used in the prediction of state variables in various machining processes and has achieved very ideal results [22]. In order to monitor the grinding temperature of Inconel718 alloy with the abrasive belt of the manipulator, Ren *et al.* (2020) proposed a modeling method of grinding temperature based on BADS-LSSVM and used the machine learning method to establish a regression model to predict the grinding temperature, and the prediction accuracy of the model reached more than 90% [23]. Konget al. (2020) proposed a prediction model of tool wear based on WOA-SVM for titanium alloy milling process and confirmed the validity of the prediction model through orthogonal experimental design and significance test [24].

Compared with the prediction of state variables in other machining processes, the relative motion between tool and workpiece becomes very complicated due to the complex natural properties and structural characteristics of SNS grinding. The theoretical method, experimental design method which need complex mathematics calculation and large quantities of experiments are not suitable for surface roughness prediction of natural stone. In this paper, an improved whale algorithm was used to optimize the internal parameters of the SVM prediction model, and a surface roughness prediction model considering the grinding complexity was constructed to effectively guide the adjustment of process parameters. This paper is organized as follows In Section 2, the traditional model of surface roughness of natural stone is given, and the collection and processing of experimental data are described. Section 3 describes the SVM theory. Section 4 introduces the basic WOA algorithm, and the SVR parameter optimization strategy based on IWOA is proposed. In Section 5, the experimental results are analyzed and discussed, and the values of MAE (1.8745) and RMSE (2.2832) obtained by IWOA-SVR model were superior to those of the SVR model optimized by GS and IWOA. Conclusions are presented in Section 6.

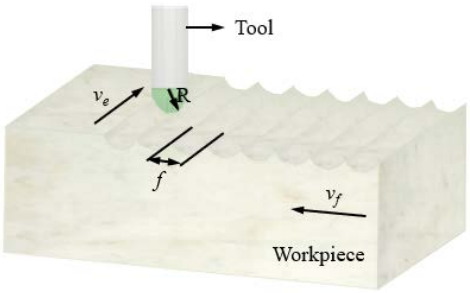

FIGURE 1. Ideal surface topography of stone grinding.

II. DEFINITION OF SURFACE ROUGHNESS OF STONE AND THE EXPERIMENTAL DATABASE

A. THEORETICAL MODEL FOR SURFACE ROUGHNESS OF NATURAL STONE

The hardness and brittleness of natural stone make it different from the grinding mechanism of metal materials, so the roughness prediction model of metal materials is not applicable to natural stone. The grinding surface roughness of stone is composed of geometric interference roughness and brittle fragmentation roughness [25]. The ideal surface topography of stone grinding is shown in Figure 1. The surface topography is a periodic circular groove and the geometric interference roughness is $R_{a,g}$. To a certain extent, the grinding surface reflects the geometric shape of the tool, which represents the interference relationship between the tool and the workpiece during grinding. The ideal surface residual profile is the basis of stone grinding surface roughness.

The geometric interference roughness of the ideal residual profile can be calculated as follows:

$$h = \frac{2r_\varepsilon - \sqrt{r_\varepsilon^2 - f^2/4}}{2} - \frac{\arcsin\left(f/2\, r_\varepsilon\right) r_\varepsilon^2}{f} \tag{1}$$

$$R_{a,g} = \frac{2}{f}\left[r_\varepsilon^2 \arccos\left(1 - \frac{h}{r_\varepsilon}\right) - (r_\varepsilon - h)\sqrt{2r_\varepsilon h - h^2}\right] \tag{2}$$

The continuous expansion of the crack will lead to the periodic fracture of the chip resulting in the uneven surface of the stone processing. The shape of the pit can be simplified to a triangle, then the theoretical value of the brittle fragmentation roughness $R_{a,b}$ is:

$$R_{a,b} = \frac{K_{IC}^{2/3}\chi^{1/3} f a_p \left(\sqrt{F_p^2 + F_c^2}\right)^{1/6}}{4\sqrt{\pi} F_c} \tag{3}$$

During the grinding process of stone, residual pits on the original ideal surface will increase the roughness and thus reduce the surface quality. The superposition of brittleness crushing roughness on geometric interference roughness is the main factor that constitutes the theoretical roughness of stone grinding. In order to simplify the problem, the following assumptions are made: the effects of tool wear, machining error and machining equipment vibration on the roughness are ignored in the grinding process; then the theoretical roughness of stone grinding R_a can be expressed as:

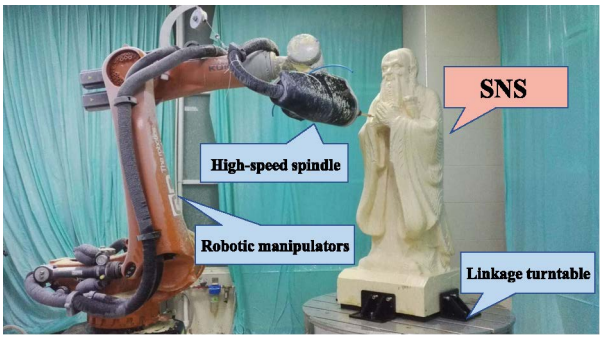

FIGURE 2. The overall structure of SNS robotic grinding system.

$$\begin{aligned} R_a &= R_{a,b} + R_{a,g} \\ &= \frac{2}{f}\left[r_\varepsilon^2 \arccos\left(1 - \frac{h}{r_\varepsilon}\right) - (r_\varepsilon - h)\sqrt{2r_\varepsilon h - h^2}\right] \\ &\quad + \frac{K_{IC}^{2/3}\chi^{1/3} f a_p \left(\sqrt{F_p^2 + F_c^2}\right)^{1/6}}{4\sqrt{\pi} F_c} \end{aligned} \tag{4}$$

Formula (4) indicates that most of the parameters in the theoretical formula of the surface roughness are related to the material properties of machined stone and the cutter, which are nonlinear and difficult to confirm. It is difficult to predict the surface roughness for natural stone with this formula in practice, so it is limited in practical applications. Notably, the parameters of the cutter when machining are important factors that can affect the surface roughness. The main goal of surface roughness prediction in natural stone grinding is to guide the optimization of machining parameters and improve the machining efficiency of robotic manipulators.

B. EXPERIMENTAL DATA ACQUISITION FOR ROBOTIC GRINDING SNS

The processing equipment used in this paper is a SNS robotic grinding system as shown in Figure 2. The hardware parts mainly include mechanical arm, electric spindle, rotary table, tool library, tool setting instrument. The system uses KUKA QUANTECK KR240 R2900 ULTRA 6-axis tandem manipulator manufactured by KUKA, Germany. The robotic manipulator belongs to KUKA's high load class equipment with a maximum motion range of 2896mm, a rated load of 240kg and a maximum load of 290kg. The repeated positioning accuracy of the manipulator is ±0.06mm and the linear trajectory accuracy is 0.031mm, which has high positioning accuracy and can meet the processing needs of large size and complex shape stone. The system is selected the Italian HSD ES747 type motorized spindle with the maximum speed of 10000 rpm, the rated power of 22kW and the rated torque of 58N·m and is equipped with ISO50 series tool holder. The diameter of the rotary table is 1520mm and the maximum vertical bearing capacity is 15T with the maximum speed of 10rpm, and the mechanical arm composed of 6+1

TABLE 1. Main mineral composition of white marble used in experiment.

Chemical Formula	Mineral Composition	Mohs Hardness	Density (g/cm³)	Crystal Form
SiO_2	Quartz	7	2.65-2.66	Hexagon
$NaAlSi_3O_8$	Normal stone	6-6.5	2.54-2.57	Monoclinic
$(Mg,Fe,Na)(Si,Al)_2O_6$	Pyroxene	5-6	3.02-3.45	Monoclinic
$KMg_3(FeSi_3O_{10})(OH)_2$	Mica stone	2.5-3	2.7-2.3	Monoclinic

shaft linkage processing system through the servo motor and reducer control and transmission.

This paper chooses white marble as the test material (800mm*600mm) that is a kind of fine marble, white color, the relatively hard texture with the general Mohs hardness of 2.5∼3.5. X-ray diffraction analyzer was used to analyze the chemical composition of the sample. It was found that the sample was composed of $NaAlSi_3O_8$,$(Mg,Fe,Na)(Si,Al)_2O_6$,$KMg_3(FeSi_3O_{10})(OH)_2$, SiO_2 and trace metals. According to the analysis of the chemical composition of white marble, the corresponding mineral composition is shown in Table 1. It can be seen that the main mineral composition of white marble selected in this paper includes quartz, normal stone, pyroxene and mica stone. The hardness of quartz, normal stone and pyroxene is high, which is the main factor affecting the surface roughness of white marble.

The surface roughness of SNS is not only affected by the different mineral composition of stone, but also can be divided into three types: grinding process parameters, tool attributes and model shape of SNS. In the grinding process of stone, grinding speed, grinding width, grinding depth and spindle speed are the most important process parameters affecting the surface roughness, so the above variables are selected as the influencing factors of the processing process parameters in this paper. Because of the hard and brittle characteristics of white marble, it is easy to cause tool wear when using carbide tools to process stone, while diamond tools have high hardness, wear resistance and corrosion resistance. Therefore, in this paper, brazed diamond taper ball head tools with radii of 2mm, 3mm and 4mm are selected to grind and finish the white marble. In the tool attributes, we only take the tool size as the influencing factor. In addition, a computational model of surface grinding complexity is proposed to quantitatively analyze the model shape of SNS.

In the actual grinding process, the influences of various factors cannot be simply linear superposition. Therefore, the following formula is used to calculate the grinding complexity C of SNS in unit of mm^{-1}:

$$C = \alpha \sum_{i=1}^{n} \beta_i c_i \tag{5}$$

In the formula, α is the surface correction coefficient and the specific calculation formula is as follows:

$$\alpha = \frac{a'}{a} \tag{6}$$

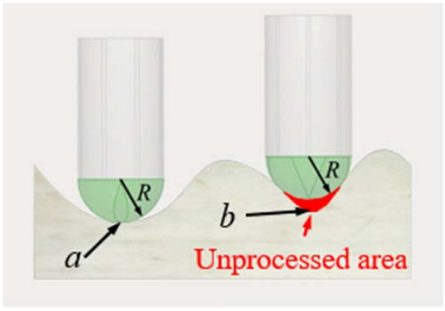

FIGURE 3. Comparison of tool radius and curvature radius.

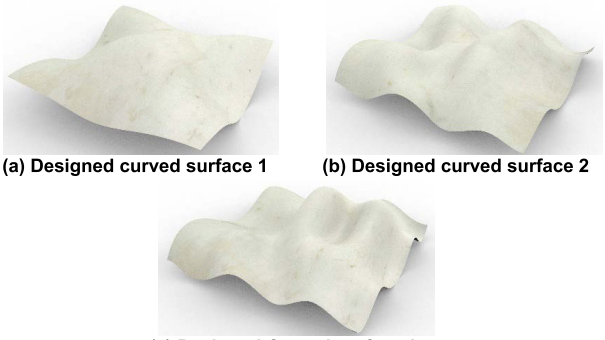

FIGURE 4. Schematic diagram of SNS curved surfaces with different grinding complexity.

In the formula, a' is the actual surface area and a is the projected surface area. The larger the surface correction coefficient is, the more complex the geometric characteristics of the surface and the more complex the grinding complexity of the surface are.

β_i is the tool diameter correction factor in the i-th subsurface. Processing surface, the relationship between the tool radius and surface curvature radius as shown in Figure 3. When using the same radius of tool machining of curved surface, due to the position a tool radius R less than the local radius of curvature of surface, so the surface at position a can be completely processed, tool radius R at position b is greater than the surface of the local radius of curvature, lead to not completely processing b surface with residuals, which affects the final machining time and surface roughness. Therefore, formula (7) is used to calculate the tool diameter correction coefficient.

$$\beta_i = \frac{D}{r^i_{\min}} = \frac{2R}{r^i_{\min}} \tag{7}$$

c_i is the geometric complexity of the i-th subsurface, which is defined as the range of the mean curvature of the subsurface. The calculation formula of c_i is as follows:

$$c_i = \left| H^i_{\max} - H^i_{\min} \right| \tag{8}$$

Three diamond taper ball-head tools with radius of $R_2 =$ 2mm, $R_3 =$ 3mm and $R_4 =$ 4mm were selected as finishing tools. The set range of spindle speed n was 7000-9000 rpm;

TABLE 2. Factor level table of finishing orthogonal test.

(a) Factor Level Table of tool R_2

Factor	Level		
	1	2	3
n /r·min-1	7000	8000	9000
f /mm·min-1	800	1000	1200
ae /mm	0.2	0.4	0.6
ap /mm	0.3	0.6	0.9
C /mm-1	0.0211	0.2448	0.4311

(b) Factor Level Table of tool R_3

Factor	Level		
	1	2	3
n /r·min^{-1}	7000	8000	9000
f /mm·min^{-1}	800	1000	1200
a_e /mm	0.2	0.4	0.6
a_p /mm	0.3	0.6	0.9
C /mm^{-1}	0.0316	0.3672	0.6466

(c) Factor Level Table of tool R_4

Factor	Level		
	1	2	3
n /r·min^{-1}	7000	8000	9000
f /mm·min^{-1}	800	1000	1200
a_e /mm	0.2	0.4	0.6
a_p /mm	0.3	0.6	0.9
C /mm^{-1}	0.4311	0.6466	0.8621

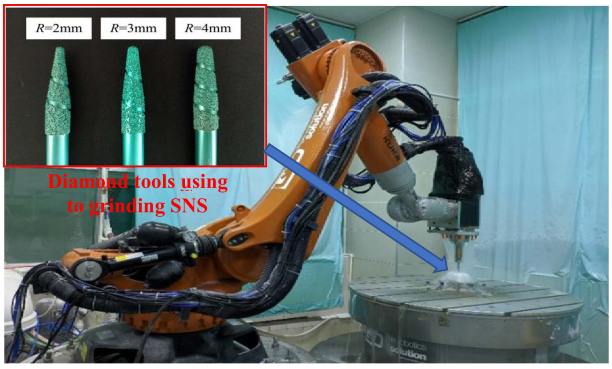

FIGURE 5. SNS finish grinding by robotic manipulators.

(a) Finishing curved surface 1

(b) Finishing curved surface 2

(c) Finishing curved surface 3

FIGURE 6. Schematic diagram of SNS finishing molding sample.

the set range of feed speed f was 800∼1200 mm/min; the set range of cutting depth a_p was 0.3∼ 0.9mm and the set range of cutting width a_e was 0.2∼ 0.6mm. Three test levels with the same interval were selected for each process parameter. The experiment selected three designed surface with different grinding complexity as shown in Figure 4, and according to the above mentioned Formula (5), surface grinding complexity due to the Formula (5) the information contained in the cutter diameter and so on the same surface, using three kinds of cutting tool processing, calculation of the surface of grinding the complexity of value is not the same, so orthogonal test design is required for each selected finishing tool. The specific parameter design is shown in Table 2.

According to the above orthogonal test table, 27 groups of tests were carried out for each tool with a total of 81 groups of tests. The grinding experiment process is shown in Figure 5. The brazed diamond ball-end tool with the 2mm, 3mm and 4mm tip radius was used in these experiments according to the curvature characteristics of samples. And the particle size of the brazed diamond also has a certain influence on the processing result. The larger the diamond particles are, the higher the grinding efficiency, but the surface quality of the white marble also decreases, so a brazed diamond tool with a diamond particle size of 30/35μm was selected according to the requirement of it. The parallel finishing milling scheme is used for machining the special-shaped stone. After machining, Mitutoyo Surftest SJ-310 surface roughness meter was used to measure the roughness value of each white marble surface. Figure 6 shows the SNS sample after finishing grinding with diamond tool.

It is obviously in Table 2, the input data vary greatly in different dimensions. In order to avoid the increase of model errors due to the large difference of data in different dimensions, it is necessary to scale data to a small interval in a certain proportion. The normalized mapping methods are often used as follows:

$$x_i^{'} = \frac{x_i - \min(x_i)}{\max(x_i) - \min(x_i)}, \quad i = 1, 2, 3 \cdots, m \tag{9}$$

where and max (x_i) and min (x_i) are the maximum and minimum number of data sequences. $x_i^{'}$ is the normalized data. x_i is the input data.

III. SUPPORT VECTOR MACHINE METHOD

A. THE BASIC THEORY OF SVM

The basic idea of SVM is to find a hyperplane that maximizes or minimizes the spacing between all samples and planes.

When SVM is used in regression analysis, its task is to minimize the spacing between the farthest sampling point and the hyperplane. Support vector machine regression (SVR) is a common model used by SVM to solve regression problems [26] and its algorithm is shown in Figure 7. In the grinding process of SNS, the input variable x_i and the output variable Ra_i of each set of experiments constitute the sample space $\{(x_i, Ra_i), i = 1, 2, 3, \cdots, n\}$. By introducing the relaxation factors ξ *and* ξ^*, Ra_i can be expressed as the following nonlinear function model:

$$\hat{y} = f(\boldsymbol{x}) = \omega^{\mathrm{T}}\boldsymbol{x} + b \tag{10}$$

Through Lagrangian construction of formula (10), the optimization problem is dualized. The formula is as follows:

$$\begin{aligned} &L(\boldsymbol{\omega}, b, \boldsymbol{\alpha}, \boldsymbol{\alpha}^*, \boldsymbol{\xi}, \boldsymbol{\xi}^*, \boldsymbol{\mu}, \boldsymbol{\mu}^*) \\ &= \frac{1}{2}\|\boldsymbol{\omega}\|^2 + C_{\mathrm{p}}\sum_{i=1}^{n}(\xi_{\mathrm{i}} + \xi_{\mathrm{i}}^*) + \sum_{i=1}^{n}\alpha_{\mathrm{i}}[f(x_{\mathrm{i}}) - y_{\mathrm{i}} - \varepsilon - \xi_{\mathrm{i}}] \\ &\quad + \sum_{i=1}^{n}\alpha_{\mathrm{i}}^*[y_{\mathrm{i}} - f(x_{\mathrm{i}}) - \varepsilon - \xi_{\mathrm{i}}^*] - \sum_{i=1}^{n}\mu_{\mathrm{i}}\xi_{\mathrm{i}} \\ &\quad - \sum_{i=1}^{n}\mu_{\mathrm{i}}^*\xi_{\mathrm{i}}^* \end{aligned} \tag{11}$$

According to the optimal conditions, take its partial derivative:

$$\begin{cases} \dfrac{\partial L}{\partial \boldsymbol{\omega}} = \boldsymbol{\omega} - \sum_{i=1}^{n}(\alpha_{\mathrm{i}}^* - \alpha_{\mathrm{i}}) = 0 \\ \dfrac{\partial L}{\partial b} = \sum_{i=1}^{n}(\alpha_{\mathrm{i}}^* - \alpha_{\mathrm{i}}) = 0 \\ \dfrac{\partial L}{\partial \xi_{\mathrm{i}}} = C_{\mathrm{p}} - \alpha_{\mathrm{i}} - \mu_{\mathrm{i}} = 0 \\ \dfrac{\partial L}{\partial \xi_{\mathrm{i}}^*} = C_{\mathrm{p}} - \alpha_{\mathrm{i}}^* - \mu_{\mathrm{i}}^* = 0 \end{cases} \tag{12}$$

Based on formula (12), the dual form of the original formula can be written as:

$$\begin{cases} \max\limits_{\alpha,\alpha^*} \sum_{i=1}^{n}[y_{\mathrm{i}}(\alpha_{\mathrm{i}}^* - \alpha_{\mathrm{i}}) - \varepsilon(\alpha_{\mathrm{i}}^* + \alpha_{\mathrm{i}})] \\ \qquad -\dfrac{1}{2}\sum_{i=1}^{n}\sum_{j=1}^{n}(\alpha_{\mathrm{i}}^* - \alpha_{\mathrm{i}})(\alpha_{\mathrm{j}}^* - \alpha_{\mathrm{j}})\boldsymbol{x}_{\mathrm{i}}^{\mathrm{T}}\boldsymbol{x}_{\mathrm{j}} \\ s.t. \begin{cases} \sum_{i=1}^{n}(\alpha_{\mathrm{i}}^* - \alpha_{\mathrm{i}}) = 0 \\ 0 \le \alpha_{\mathrm{i}}, \alpha_{\mathrm{i}}^* \le C_{\mathrm{p}} \end{cases} \end{cases} \tag{13}$$

The above calculation process needs to meet Karush-Kuhn-Tucker (KKT) condition and the final solution is in the form of:

$$f(\boldsymbol{x}) = \sum_{i=1}^{n}(\alpha_{\mathrm{i}}^* - \alpha_{\mathrm{i}})\boldsymbol{x}_{\mathrm{i}}^{\mathrm{T}}\boldsymbol{x} + b \tag{14}$$

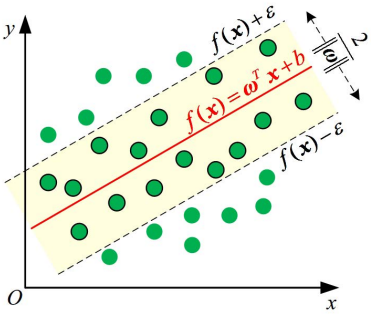

FIGURE 7. Schematic diagram of the SVR regression process.

If it is nonlinear, kernel function $K(\boldsymbol{x}_{\mathrm{i}}, \boldsymbol{x}_{\mathrm{j}})$ can be introduced and the model of SVR under nonlinear condition can be obtained as follows:

$$f(x) = \sum_{i=1}^{n}(\alpha_{\mathrm{i}}^* - \alpha_{\mathrm{i}})K(\boldsymbol{x}_{\mathrm{i}}, \boldsymbol{x}_{\mathrm{j}}) + b \tag{15}$$

Kernel $K(x_{\mathrm{i}}, x_{\mathrm{j}})$ is one of the core parts of support vector machines and its essence is the inner product in feature space. The functions of Kernel are to represent samples from original space to higher-dimensional space, so that they become linearly separable data and reduce the complexity of operation. The feature spaces mapped by different kernel functions are also highly different. The Gaussian radial basis function, which is characterized by high adaptability, is selected as the kernel function in this paper, as shown in formula (16):

$$K(x_i, x_j) = \exp\left(-\frac{\|x_i - x_j\|}{2g^2}\right) \tag{16}$$

B. PARAMETER SELECTION FOR SVR THEORY

In the SVR algorithm, the precision of the model is sensitive to the penalty factor C_{p} and the kernel width g in the Gaussian Kernel function. Penalty factor C_{p} said sample points on the weight of the sample size from the group, when C_{p} to take larger value indicating that samples have bigger influence on the objective function from the group, so the SVR model is trained on the sample data of the control more strictly; the final fit degree of the predicted values and measured values will be better; but if the C_{p} is too big, model in training degree of punishment is too big with an overfitting problem; if C_{p} is set to a smaller value, the complexity of SVR model operation will be reduced, but the final fit of the model will also be reduced resulting in the accuracy of the model failing to meet the requirements. The distribution features of training samples in the high-dimensional feature space are mainly determined by the kernel width g. When g is too small, the relationship between each support vector will become relaxed and the generalization ability of the trained model is too poor to be used for prediction. On the contrary, if the value of g is too large, then the influence between support vectors is too strong, resulting in insufficient accuracy. Therefore, reasonable selection of C_{p} and g is of great significance for establishing SVR prediction model. In order to study the

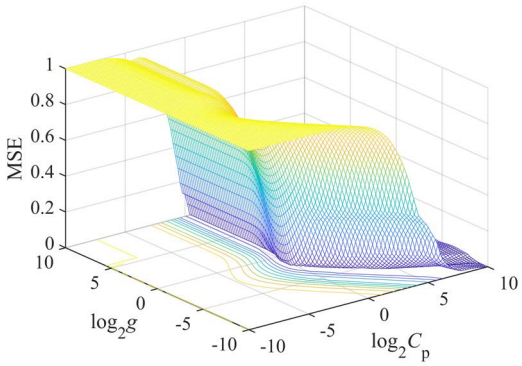

FIGURE 8. Influence of C_p and g on SVR model accuracy.

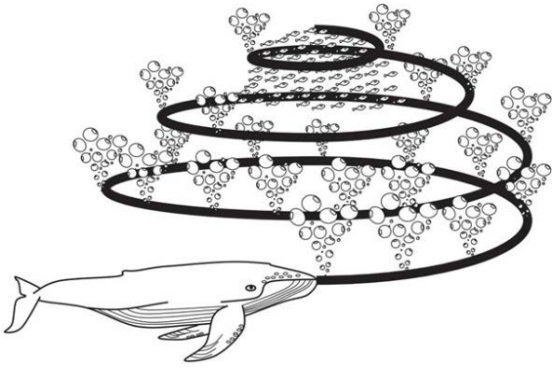

FIGURE 9. Bubble net hunting behavior of humphead whales.

influence of C_p and g on the prediction results under the data set conditions in this paper, 20 groups were randomly selected as the training set by using the data of orthogonal test of cutting tools with a radius of 2mm. The value ranges of C_p and g were set as [0, 100], and the prediction accuracy of the model was reflected by root mean square error (MSE). The relationship diagram of MSE changing with (C_p, g) was drawn as shown in Figure 8. It can be seen from the figure that the selection of internal parameter (C_p, g) value of SVM determines the prediction performance of the model.

The optimal algorithms for SVR parameters can be divided into two categories: numerical algorithms and heuristic algorithms. Numerical algorithms need to traverse a specific search space to find appropriate parameters, so the search efficiency is low. Once Tan et al used the grid search algorithm (GS) in numerical algorithms to optimize the internal parameters of SVR [27]. Compared with numerical algorithms, heuristic algorithms such as ant colony optimization algorithm, Biogeography based optimization algorithm and Particle swarm based optimization algorithm, etc., firstly take a random position in the state space as the starting point of search, and evaluate each position to be searched. The current good position is obtained by comprehensive evaluation results and then the search is continued from the current good position until the final target is found. The model has higher accuracy and faster calculation speed. Whale optimization algorithm (WOA) is a heuristic search algorithm proposed by Mirjalili in 2016. Compared with other heuristic search algorithms, this algorithm is not only simple in principle and easy to understand, but also requires fewer parameters to be manually set and it has certain advantages in terms of algorithm operation speed. In this paper, logarithmic weight factor and random differential variation strategy were introduced to optimize the SVR parameters based on the whale algorithm proposed by Mirjalili, so as to realize the accurate prediction of the surface roughness in the process of grinding SNS by robotic manipulator.

IV. OPTIMIZATION OF SVR WITH IWOA

A. BASIC WOA ALGORITHM

The generation of the WOA algorithm is inspired by the special bubble net hunting method of humpback whales. When hunting, humpback whales chase prey near the surface by creating unique bubbles along the spiral or inverted triangular path shown in Figure 9. The WOA algorithm mainly includes the following three parts:

1) Encircling Prey

The whale groups will first identify the location of the prey and then try to encircling the prey. The WOA algorithm will assumes the target prey or prey near the target to be current optimal. After defining the current optimal prey, other whale individuals in the population will change their location. This procedure can be represented by the following formula:

$$\vec{D} = \left| \vec{C} \cdot \vec{X^*}(t) - \vec{X}(t) \right| \tag{17}$$

$$\vec{X}(t+1) = \vec{X^*}(t) - \vec{A} \cdot \vec{D} \tag{18}$$

Among them, the vectors $\vec{A}$ and $\vec{C}$ are calculated by the following formula:

$$\vec{A} = 2\vec{a} \cdot \vec{r} - \vec{a} \tag{19}$$

$$\vec{C} = 2 \cdot \vec{r} \tag{20}$$

In the formula, the $\vec{r}$ is the vectors uniformly distributed on the [0,1] and the $\vec{a}$ is a convergence factor. Its expression is:

$$\vec{a} = 2 - \frac{2t}{T_{\max}} \tag{21}$$

In the formula, the t represents the current number of the iterations; the $T_{\max}$ represents the maximum number of the iterations and the $\vec{a}$ decreases linearly from 2 to 0.

2) Bubble-Net Attacking Method The whales approach their prey in a spiral upward motion, and encircling it up by gradually narrowing the circle of the encirclement. This process was modeled by the two methods: the shrinking encircling mechanism and the spiral updating position. Among which, the modeling of shrinkage encirclement process can be implemented by reducing the value of the $\vec{a}$ in formula (21). The process of the spiral updating position is calculated by the following formula:

$$\vec{X}(t+1) = \vec{D'} \cdot e^{\mathrm{bl}} \cdot \cos(2\pi l) + \vec{X^*}(t) \tag{22}$$

The $\vec{D'}$ is calculated by the following formula:

$$\vec{D'} = \left| \vec{X^*}(t) - \vec{X}(t) \right| \tag{23}$$

To simulate both behaviors simultaneously, the probability of selecting both methods is assumed to be 50%, then the mathematical model of the process of Bubble-Net Attacking Method is as follows:

$$\overrightarrow{X}(t+1) = \begin{cases} \overrightarrow{X^*}(t) - \overrightarrow{A} \cdot \overrightarrow{D} & p < 0.5 \\ \overrightarrow{D'} \cdot e^{\mathrm{bl}} \cdot \cos(2\pi l) + \overrightarrow{X^*}(t) & p \geq 0.5 \end{cases} \quad (24)$$

3) Search for Prey

When the coefficient vector $\left|\overrightarrow{A}\right| > 1$, it means that the whale is swimming outside the circle of the contractive encirclement, the position of the partner affects the position of the individual of the peripheral whale in this case and the peripheral whales randomly search prey within the area, instead of choosing the currently optimal whale location for proximity. Its mathematical model is:

$$D = \left|\overrightarrow{C} \cdot \overrightarrow{X_{\mathrm{rand}}} - \overrightarrow{X}\right| \quad (25)$$

$$\overrightarrow{X}(t+1) = \overrightarrow{X_{\mathrm{rand}}} - \overrightarrow{A} \cdot \overrightarrow{D} \quad (26)$$

B. WOA WITH DIFFERENTIAL MUTATION STRATEGY

Although the principle of WOA algorithm is simple and easy to understand, it has a few parameters needed to manually adjust the set and certain advantages in algorithmic operation speed aspect. From the principle of WOA algorithm, its optimization needs to balance local development with global search ability just like other algorithms, that is, through the size of the $\overrightarrow{A}$ parameters to coordinate. It can be seen from formula (19) that the change of the value of the control parameter $\overrightarrow{A}$ depends on the change of the parameter $\overrightarrow{a}$, that is, the smaller the value $\overrightarrow{a}$, the stronger the local development ability of the algorithm; the larger the value $\overrightarrow{a}$, the stronger the global search ability of the algorithm. The $\overrightarrow{a}$ is the parameter that linearly decreases from 2 to 0 in the iterative search. However, the control factor $\overrightarrow{a}$ can't be satisfied by linearly decreases law in the actual complex function optimization, which easily leads to the algorithm is difficult to jump out of the local optimal, and the optimization effect is poor. For this deficiency, we introduce a positive tangent nonlinear control factor and its specific expression is:

$$\overrightarrow{a} = 2 - 2\tan\left(\frac{\pi t}{4T_{\max}}\right) \quad (27)$$

From formula (27), it can be seen that the value of the $\overrightarrow{a}$ starts decrease at a relatively slow speed from 2 in the early iteration process which is conducive to carry out the sufficient global search. But the decreases speed of the value $\overrightarrow{a}$ is significantly accelerated in the later iteration process, which is conducive to the local search and accelerates the convergence speed.

When the weight factor is large, its search range is relatively large, which is conducive to the global search; while its value is small, a high-precision search can be performed in a small range. To enhance the optimization ability of the whale optimization algorithm, adaptive weight factors $w(t)$ with logarithmic change rules are introduced to update the algorithm position to update the algorithm location. The weight position adjustment mathematical model is:

$$\overrightarrow{X}(t+1) = \begin{cases} \overrightarrow{X^*}(t) - w(t)\,\overrightarrow{A} \cdot \overrightarrow{D} & p < p^* \\ \overrightarrow{X^*}(t) + w(t)\,\overrightarrow{D}\,e^{bl}\cos(2\pi l) & p \geq p^* \end{cases} \quad (28)$$

In the formula, the p is the random number between the [0, 1]; The value of the p^* is 0.5; the mathematical expression for the adaptive weight factor is as follows:

$$w(t) = e^{-(10t/T_{\max})^2} \quad (29)$$

From formula (29), it can be seen that the value of the $w(t)$ is larger indicating that the step length value participating in the position adjustment is large in the early iteration process and the algorithm has strong global exploration ability. At the later stage of the iteration, the value of the $w(t)$ is getting smaller and close to zero and the local search ability of the algorithm is getting stronger and stronger.

According to the principles of the basic whale optimization algorithm, in the optimization process, the current individual will change its position according to the distance between the optimal individual position and itself, and other non-current optimal individuals will gradually approach to the optimal individual position. This updating method has some drawbacks. When the position of the current optimal individual is not globally optimal, all individuals in the population will be misguided to gather near the local optimal area with the number of iterations increases, which made the diversity of the population decreases resulting in premature convergence of the algorithm and low optimization accuracy. For this problem, the IWOA algorithm draws the advantages of differential variation strategies in differential evolutionary algorithms, integrating the stochastic difference variability strategy into the basic whale algorithm, that is, the randomly selected individuals and the current optimal individuals in the population make random difference with the current individual respectively to generates the new individuals. Increasing the diversity of population individuals is to prevent the algorithm from falling into local optimal due to premature convergence.

The expression for the random difference variation is:

$$\overrightarrow{X}(t+1) = u\left[\overrightarrow{X^*}(t) - \overrightarrow{X}(t)\right] + u\left[\overrightarrow{X'}(t) - \overrightarrow{X}(t)\right] \quad (30)$$

The IWOA algorithm performs search tasks starting with a set of random solutions. throughout the search, the whale updates its position based on either the current optimal target position (the phase of the Bubble-Net Attacking Method) or in according with a randomly selected target position (the phase of the random search for prey), ends the search if the termination criteria are met. Because the method introduced logarithmic weight factor and random differential variation strategy on the basis of the ordinary whale algorithm, it has enhanced the algorithm coordination performance between global search and local development and the ability for avoid falling into the local optimal.

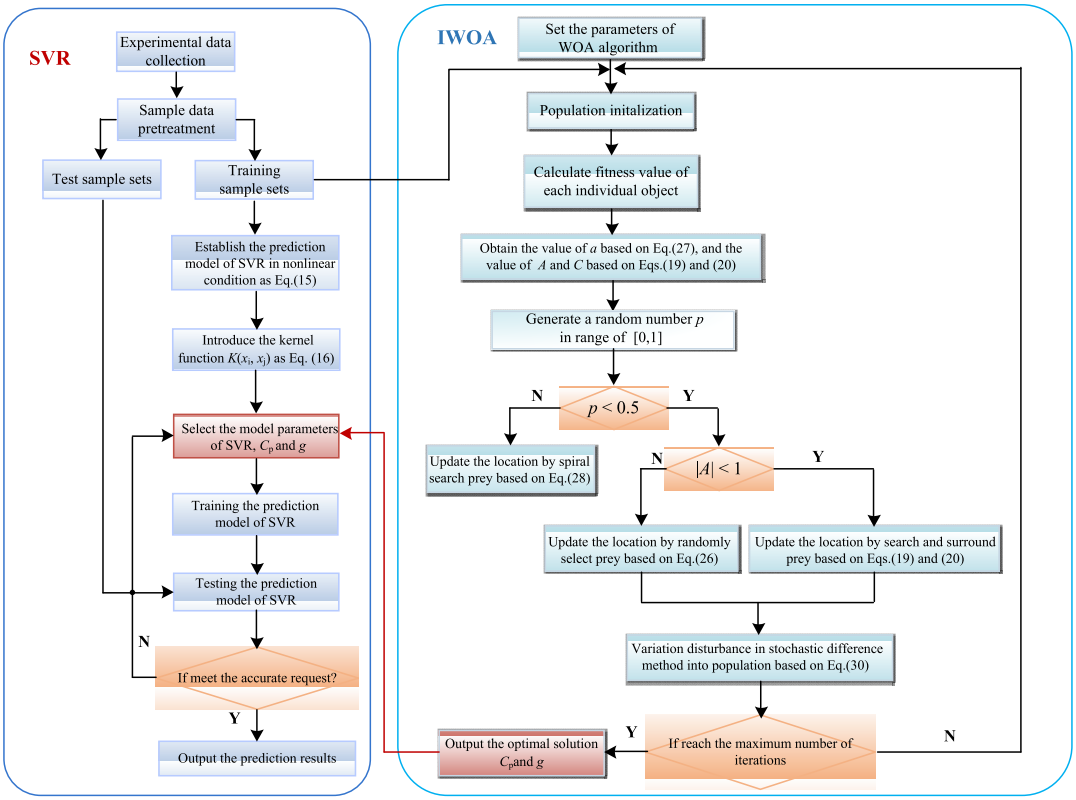

FIGURE 10. Modeling flow diagram of IWOA-SVR.

C. STRATEGY OF IWOA WITH SVR

According to the IWOA algorithm process, setting reasonable parameters and using IWOA algorithm can optimize the penalty factor C_p in the SVR model and the width g in the Gaussian kernel function, it adopted the IWOA-SVR to establish a modeling process for the SNS surface roughness as shown in Figure 10. The specific steps can be summarized as follows:

Step 1: To eliminate the impact of the scale, it first needs to conduct the naturalization of the test data.

Step 2: The processed sample data is divided in a certain proportion into the training set and the test set two parts.

Step 3: Adopt IWOA algorithm to conduct an iterative search for the optimal combination of SVR model parameters (C_p, g) within a specified range. Parameter combination (C_p, g) represents the location of each individual whale (i.e. a feasible solution). The search direction is determined by the fitness function using the results and number of iterations to determine whether the iteration is stopped.

Step 4: Use the optimized parameter combination (C_p, g) to establish SVR prediction model and use the model for the prediction of the SNS surface roughness.

V. EXPERIMENTAL RESULTS AND ANALYSIS

A. PERFORMANCE CRITERIA

To allow a fair comparison of the algorithms to be made, root mean square error (RMSE), mean absolute error (MAE), and mean absolute percentage error (MAPE) were used to evaluate the predictions of the models. MAE, RMSE and MAPE can be calculated by the following formula:

$$\mathrm{MAE} = \frac{1}{n}\sum_{i=1}^{n}\left|y_i - y_i^*\right|$$

$$\mathrm{MAPE} = \sum_{i=1}^{n}\left(\frac{y_i - y_i^*}{y_i}\right) \times \frac{100}{n}$$

$$\mathrm{RMSE} = \sqrt{\frac{\sum_{i=1}^{n}(y_i - y_i^*)}{n}}$$

Furthermore, when splitting the dataset, a fixed ''random_state'' was used to ensure that the datasets (training set and testing set) were consistent every time. Under the condition that the randomly partitioned datasets were consistent, the parameters of each method were tuned to ensure that the algorithm comparisons were as fair as possible.

B. COMPARATIVE ANALYSIS OF THE PREDICTION PERFORMANCE

Seven groups of data were randomly selected as the test data from the model, and the IWOA-SVR, WOA-SVR in Ref [26] and GS-SVR in Ref [27] proposed in this paper were used to predict the established model. The total number of population individuals of the three algorithms is set to 40, the

TABLE 3. C_p and g values of the prediction model.

Models	GS-SVR			WOA-SVR			IWOA-SVR		
	R2	*R3*	*R4*	*R2*	*R3*	*R4*	*R2*	*R3*	*R4*
Penalty parameter C_p	18.1	52.4	16.5	2.36	65.2	126	1.78	72.4	136
Kernel width g	0.13	1.36	2.37	0.01	0.04	0.37	0.02	1.29	0.15

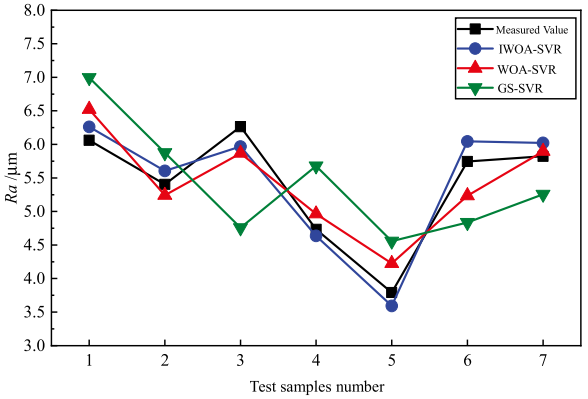

FIGURE 11. Surface roughness effect of three models on test samples.

maximum number of iterations is 100, and Gaussian radial basis function is selected as the kernel of the support vector machine regression model. After optimization iteration of each model, the final SVR parameters combination of C_p and g are shown in Table 3.

Figure 11 shows that the three models are trained on the same training set and the predict results on the same test set. From Figure 11, it can be seen that all the three models have achieved accurate prediction of SNS surface roughness and the predicted value fits well with the actual value. The stone surface roughness prediction model proposed based on the IWOA-SVR in this paper has a better prediction accuracy relative to the prediction models established based on WOA-SVR and GS-SVR. By analyzing the prediction results of 7 samples of white marble in the test set, it is found that the convexity prediction value errors are all within $-0.2 \sim 0.2$um, then the surface roughness hit rate within $-0.1 \sim 0.1$um is 91.3%. In general, the training set data is used for model building and the test set data is not participate in the parameter tuning during model building process, so the predictions on the test set can better reflect the overall performance of the model.

In order to quantitatively analyze the differences between each model, we hereby draw the regression effects of the three models on the training set and the test set as shown in Figure 12. As it can be seen from Figure 12, the regression scatter points on the test set are more evenly distributed on both sides of line $y = x$ after the model optimized by IWOA and WOA algorithm. This means that on the whole, the difference between the predicted value and the actual value is smaller and the predicted outlier is less than that of the model

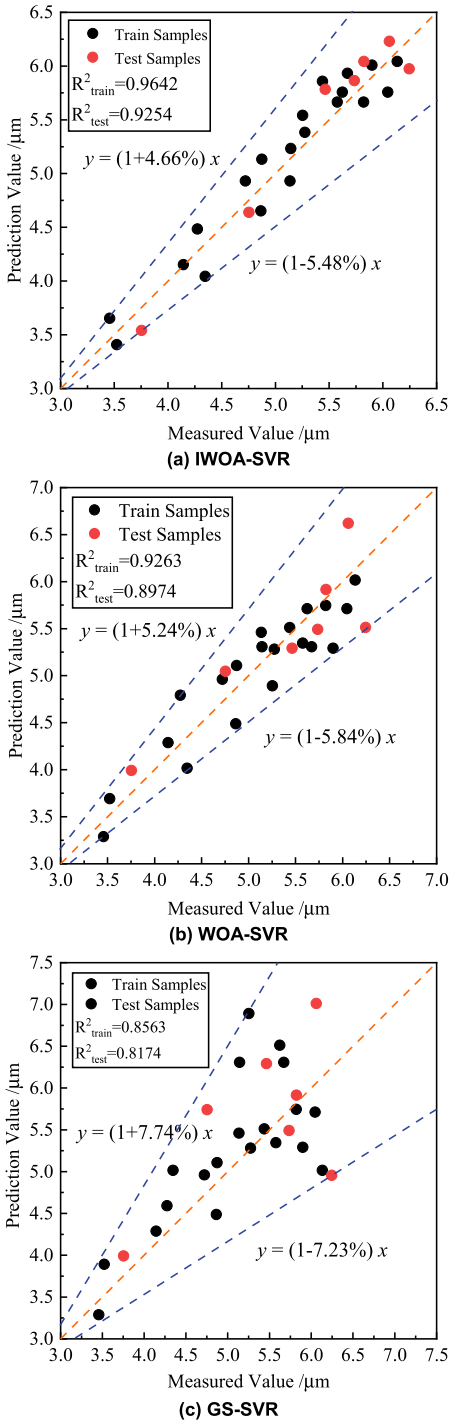

FIGURE 12. Regression effects of three models.

optimized by GS algorithm. The determination coefficient R^2 is used to evaluate the fitting degree between the predicted value and the actual value of the model. $R^2 = 1$ represents the ideal fitting state. The smaller the R^2 value, the worse the comprehensive performance of the model. The coefficient of determination of IWOA-SVM model on the training set is $R^2 = 0.9642$, and that on the test set is $R^2 = 0.9254$. Both of them are the maximum of the three models and the fitting degree is the best.

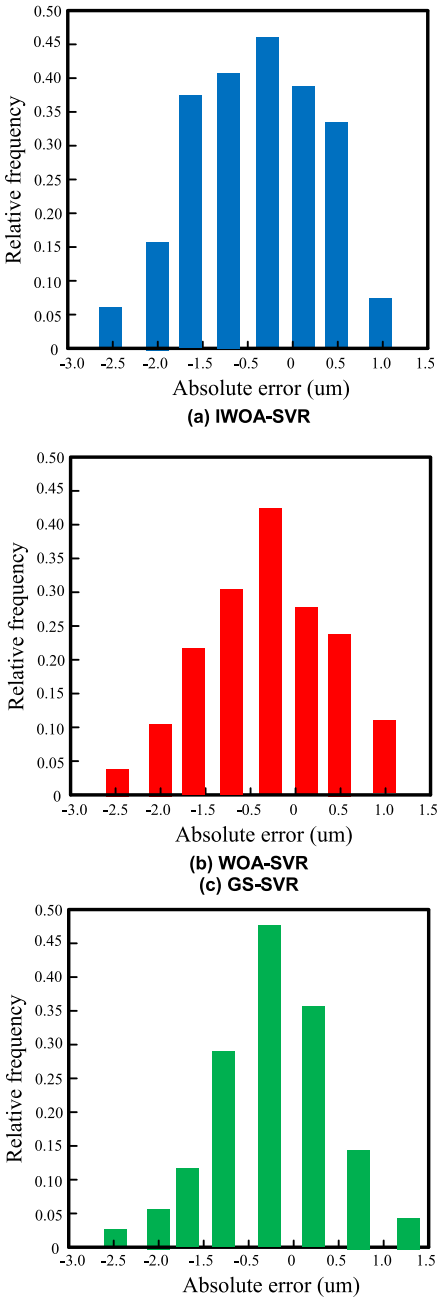

FIGURE 13. Error histograms for prediction of three models.

The absolute error distribution is also an important factor to evaluate the comprehensive performance of the model. Figure 13 is the histogram of the absolute error frequency distribution of the three models on the test set. As it can be seen from Figure 13, the absolute errors of the three models are mainly distributed between −10um and 10um, and the GS-SVR model also has a small number of abnormal samples distributed outside this range but the other two models did not, which shows that the absolute error distribution of SVR model after optimization by the heuristic intelligent algorithm WOA is more stable. Int terms of two models WOA-SVR and IWOA-SVR, the number of samples near the absolute error

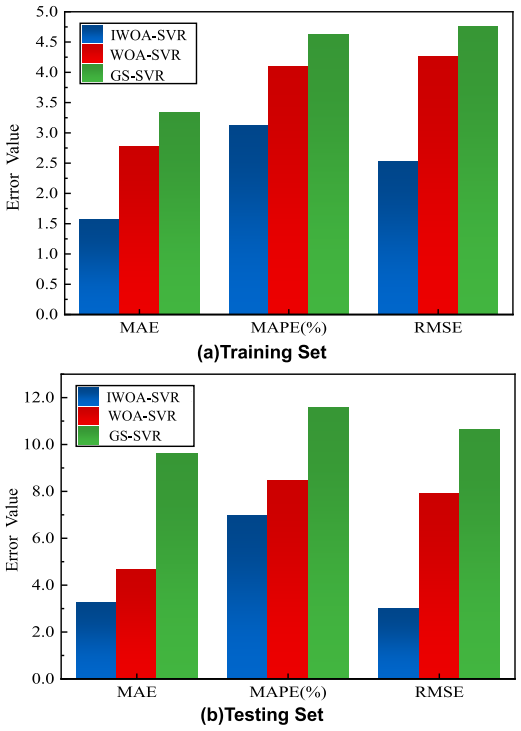

FIGURE 14. Error histogram of training set and testing set.

TABLE 4. Error index calculation value of three models for training and test set.

Algorithm	Training Set				Testing Set			
	MAE	MAPE [%]	RMSE	*t*/s	MAE	MAPE[%]	RMSE	*t*/s
IWOA-SVR	1.8745	3.3636	2.2832	31.342	3.7536	4.7863	3.7372	0.0832
WOA-SVR	2.5428	3.5107	2.9443	68.727	4.0295	5.5621	4.2881	0.1256
GS-SVR	3.3264	4.2654	3.3445	80.321	8.6654	10.105	7.6231	0.3287

of 0 of the latter is larger than that of the former. The absolute error distribution is high in the middle and low on both sides. The population error is approximately normally distributed. This also proves that IWOA-SVR model has higher fitting accuracy than WOA-SVR model.

In order to evaluate the comprehensive performance of the three surface roughness prediction models more comprehensively, three error indexes of MAE, MAPE and RMSE were selected as evaluation indexes for analysis. The error bar chart is shown in Figure 14 and Table 4 lists the calculation results of each error index. The training time of the model is related to the computational efficiency of practical application and the characteristic of less time consuming is particularly important for industrial control. Therefore, CPU time is an important indicator to judge whether the model has the potential of online application in the process of establishing the model and realizing the predicted output. In order to illustrate this problem, the training time consumed by the three models under the same iteration condition is also compared in Table 4.

According to the chart, the IWOA-SVR, WOA-SVR and GS-SVR can capture well the actual measurement trends. Among them, the predicted curve obtained by IWOA-SVR and WOA-SVR models is closer to the actual curve. Compared with the numerical GS-SVR model, the WOA-SVR adopts a heuristic algorithm and IWOA-SVR surface roughness prediction models obtained higher determination coefficient and lower error values in both the training set and the test set. It should be pointed out that due to the improvement of IWOA algorithm in local coordination ability and compared with the WOA algorithm, the MAE errors in training set and test set are reduced by 43.13% and 30.77% respectively; the MAPE errors are reduced by 23.78% and 17.39% respectively; and the RMSE errors are reduced by 40.79% and 62.18% respectively. In conclusion, the IWOA-SVM model proposed in this paper has the best generalization capability in terms of the SNS surface roughness prediction. In addition, the IWOA-SVM modeling method also has certain advantages in the computational speed. All three methods of similar prediction are implemented by Matlab2016b programming and the time spent for training and prediction on the same computer is as shown in Table 4. At the number of iterations of 100, the IWOA-SVR modeling method trains time consuming 31.342s with a predicted time consuming of 0.0832s. The training time of WOA-SVR modeling method is 68.727s and the prediction time is 0.1256s. The training time of GS-SVR modeling method is 80.321s and the prediction time is 0.3287s. It can be seen that random differential variation strategy is introduced into IWOA algorithm, which effectively avoids the phenomenon of falling into local optimization, greatly reduces the training time of the model and has excellent real-time performance.

C. ANALYSIS OF THE INFLUENCE LAWS OF THE PROCESS PARAMETERS AND GRINDING COMPLEXITY ON SURFACE ROUGHNESS

Accurate prediction of surface roughness in SNS grinding by IWOA-SVM model, which can judge in advance whether the surface roughness value of stone meets the requirements of actual production. Meanwhile, the relationship between processing parameters and surface roughness can be obtained under the different grinding complexity. In the actual processing process, the processing parameters can be retroactively traced by the predicted surface roughness value and its correlation with the processing parameters to carry out the optimization of the processing parameters, improve the surface roughness of the SNS and keep the quality of the processing process stable.

Based on the IWOA-SVM model of SNS grinding processing, the relationship between the selected processing parameters and grinding complexity and surface roughness were established. When the grinding depth, spindle speed and grinding complexity are fixed, the effect of the feeding speed and grinding width on the surface roughness is as shown in Figure 15. As it can be seen from Figure. 15, the feeding speed

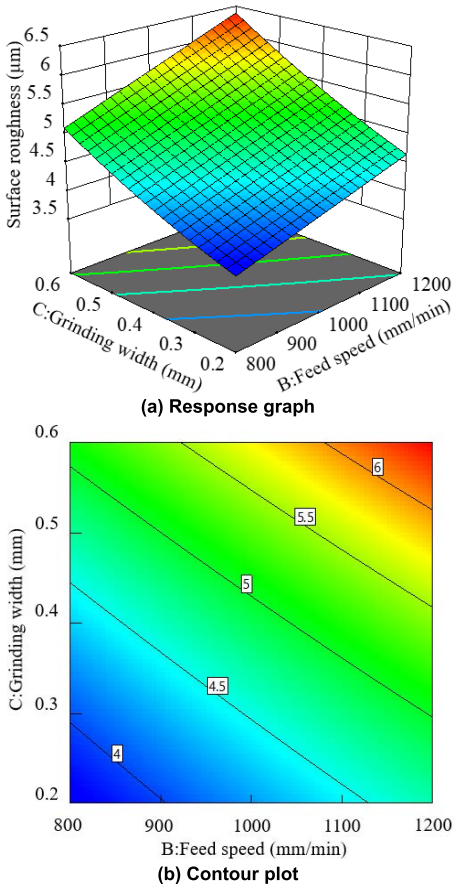

FIGURE 15. Influence of a_e and f on surface roughness.

and grinding width have significant effects on the surface roughness. The higher the feed speed, the greater the surface roughness and the surface roughness increases with the grinding width increasing. This is because the number of diamond particles involved in machining on the workpiece per unit length decreases with the increase of the feeding speed resulting in the increase of the interference of abrasive particles on the workpiece surface and the increase of the maximum undeformed thickness of a single abrasive particle leads to the increase of the surface roughness of the workpiece. When other parameters remain unchanged, increasing the cutting width leads to the increase of residual height, the increase of surface roughness and the decrease of workpiece surface quality. According to Figure 16, when the grinding depth changes within the selected range, the surface roughness changes very little. It indicates that the abrasion depth affects surface roughness within a given range of parameters, but the surface roughness increases slightly with the increase of the spindle speed, which is due to the linear velocity of the tool increases as the spindle speed increases. When other processing conditions remain unchanged, the number of abrasive particles processed per unit time increases resulting in a decrease in the maximum undeformed thickness of a single abrasive particle. And the friction force of the contact surface

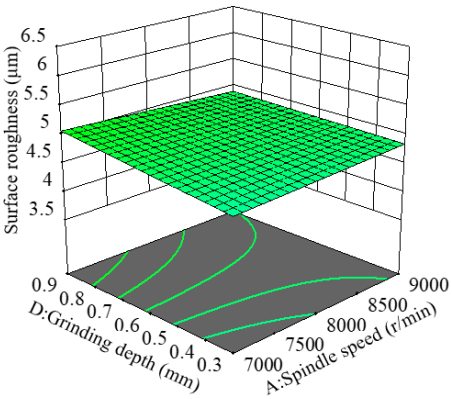

(a) Response graph

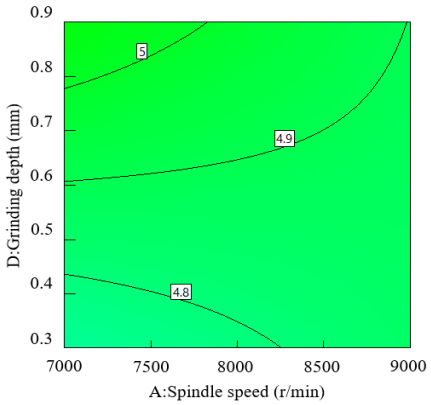

(b) Contour plot

FIGURE 16. Influence of n and a_p on surface roughness.

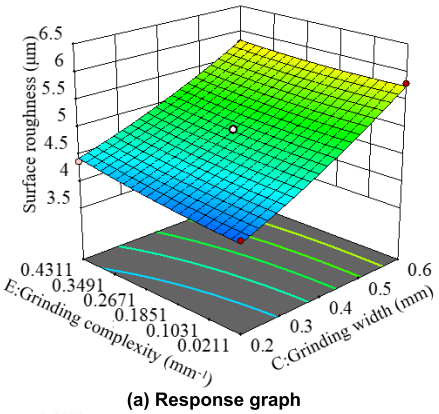

(a) Response graph

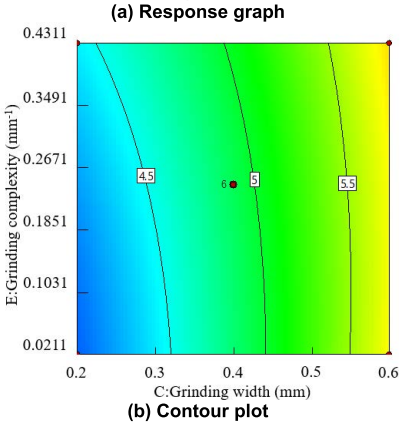

(b) Contour plot

FIGURE 17. Influence of a_e and C on surface roughness.

between the tool and the workpiece will be reduced resulting in a decrease in surface roughness. When other parameters are fixed, the influence of grinding width and grinding complexity on surface roughness is shown in Figure 17. As it can be seen from Figure 17, with the increase of surface grinding complexity, the curvature characteristics of stone surface become more complex and machining is easy to have some less cutting positions, which will lead to the increase of surface roughness. Moreover, the influence of surface grinding complexity on surface roughness is greater than that of spindle speed and cutting depth.

From the analysis of the correlation between processing parameters and surface roughness, with the selection of the higher spindle speed and the lower feed speed and the grinding width within the appropriate range, a good surface roughness can be obtained in the grinding process of SNS. In the actual selection, the intelligent parameter selection can be realized based on a given target task and the process of selecting its processing parameters is similar to that found under a single objective, that is, the correlation between each object and the processing parameters is obtained through the corresponding prediction model. Then it selects the processing parameters that meet the given requirements based on the comprehensive analysis of the correlation relations.

VI. CONCLUSION

1) The current Whale Optimization Algorithm (WOA) has several drawbacks, such as slow convergence, low solution accuracy and easy to fall into the local optimal solution. To overcome these drawbacks, an improved Whale Optimization Algorithm (IWOA) is proposed in this study. IWOA can enhance the global search capability by two measures

2) It selected Improved whale optimization algorithm (IWOA) to optimize the internal parameters of the support vector machine model (SVR) and form IWOA-SVR model, adopted the IWOA-SVR model to construct the surface roughness prediction model in the SNS mechanical arm grinding process and compared with the prediction models built by other two support vector optimization algorithms (WOA-SVR and GS-SVR). The results shown that the IWOA-SVR model can more accurately predict the surface roughness of the SNS. The predictive accuracy indicators MAE, MAPE and RMSE on the test set reached 3.7536, 4.7863 and 3.7372, respectively. It also verify that relative WOA algorithm and GS algorithm, the IWOA algorithm has the advantages of strong optimization ability and short training time.

3) Based on the effective surface roughness prediction model constructed by IWOA-SVR model, the influence of processing parameters and grinding complexity on surface roughness was further explored and the correlation diagram of influencing parameters and target variables was

constructed. It can realize the reverse trace of surface roughness, to guide the adjustment of processing technological parameters and improve the surface quality of SNS grinding processing.

ACKNOWLEDGMENT
The authors would like to thank the sponsor for this support.

DECLARATIONS
Additional declarations for articles in life science journals that report the results of studies involving humans and/or animals Not applicable.

ETHICS APPROVAL
The work was original research that has not been published previously, and not under consideration for publication elsewhere, in whole or in part.

CONSENT TO PARTICIPATE
The authors all approved to participate.

CONSENT FOR PUBLICATION
It is approved by all authors for publication.

CONFLICT OF INTEREST
The authors declare No competing interests.

NOMENCLATURE

r_ε	The radius of the tool arc/mm.
f	The feed rate of the tool/ mm·min^{-1}.
h	The height of the center line of the residual profile/mm.
a_P	Is the grinding depth/mm.
K_{IC}	Is the fracture toughness of the stone.
χ	Is the fixed coefficient related to the Poisson's ratio of the material.
F_c	Main cutting force/N.
F_c	Cutting depth resistance./N.
D	Tool diameter/mm.
R	Tool radius/mm.
$r^i_{\min}$	Minimum radius of curvature of the i-th subsurface/mm.
$H^i_{\max}$	Maximum mean curvature of the i-th subsurface.
$H^i_{\min}$	Minimum mean curvature of the i-th subsurface.
SVR	Support vector machine regression.
IWOA-SVR	Improved whale optimization algorithm.
GS	Grid-search optimization algorithm.
WOA	Whale optimization algorithm.
$\boldsymbol{\omega}$	Normal vector.
$\boldsymbol{x}$	Input vector.
$\boldsymbol{y}$	Actual value of surface roughness/um.
$\hat{\boldsymbol{y}}$	Predicted value of surface roughness/um.
ε	Insensitive loss function error.
ξ_i and ξ_i^*	Two relaxation factors.
C_p	Penalty factor.
t	Current iteration.
$\overrightarrow{A}$ and $\overrightarrow{C}$	Coefficient vector.
$\overrightarrow{X^*}$	Optimal position vector of the optimal whale by far.
$\overrightarrow{X^*}$	Will be updated in each iteration.
$\overrightarrow{X}$	Position vector of the current whale.
b	A constant that defines the spiral line.
l	A random value in [−1,1].
$\overrightarrow{D'}$	The distance of the i whale to the prey, that is the current optimal solution.
p	A value of the random distribution on the interval [0, 1].
$\overrightarrow{X_{\text{rand}}}$	Randomly selected position vector of the humpback whale.
g	Width of the kernel function
$\overrightarrow{X'(t)}$	Position vector of the individual is randomly selected.
n	Number of sample sets.
y_i	Measured value.
y_i^*	The predicted value.

REFERENCES

[1] T. Shaked, K. L. Bar-Sinai, and A. Sprecher, "Adaptive robotic stone carving: Method, tools, and experiments," *Autom. Construct.*, vol. 129, Sep. 2021, Art. no. 103809.
[2] P. Dong, J. Zhang, C. Ouyang, D. Sun, and J. Wu, "Investigation on sawing performance of diamond frame saw based on reciprocating swing in processing hard stone," *J. Mater. Process. Technol.*, vol. 295, Sep. 2021, Art. no. 117171.
[3] F.-C. Yin, Q.-Z. Ji, and C.-Z. Wang, "Research on machining error prediction and compensation technology for a stone-carving robotic manipulator," *Int. J. Adv. Manuf. Technol.*, vol. 115, pp. 1683–1700, May 2021.
[4] F.-C. Yin, "A partitioning grinding method for complex-shaped stone based on surface machining complexity," *Arabian J. Sci. Eng.*, vol. 10, no. 1, pp. 62–81, Oct. 2021.
[5] T. Wang, L. Zou, Q. Wan, X. Zhang, Y. Li, and Y. Huang, "A high-precision prediction model of surface roughness in abrasive belt flexible grinding of aero-engine blade," *J. Manuf. Processes*, vol. 66, pp. 364–375, Jun. 2021.
[6] A. Haja Maideen, M. Duraiselvam, and M. Varatharajulu, "Surface modification of aluminium 7075 by electrical discharge alloying and influence of surface roughness using RSM," *Mater. Today, Proc.*, vol. 39, pp. 1440–1449, Jan. 2021.
[7] D. Y. Pimenov, A. Bustillo, S. Wojciechowski, V. S. Sharma, M. K. Gupta, and M. Kuntoğlu, "Artificial intelligence systems for tool condition monitoring in machining: Analysis and critical review," *J. Intell. Manuf.*, vol. 1, pp. 1–18, Mar. 2022.
[8] Y. Wang, Y. Liu, X. Chu, Y. He, and W. Zhang, "Calculation model for surface roughness of face gears by disc wheel grinding," *Int. J. Mach. Tools Manuf.*, vol. 123, pp. 76–88, Dec. 2017.
[9] C. Dai, Z. Yin, P. Wang, Q. Miao, and J. Chen, "Analysis on ground surface in ultrasonic face grinding of silicon carbide (SiC) ceramic with minor vibration amplitude," *Ceram. Int.*, vol. 47, no. 15, pp. 21959–21968, Aug. 2021.
[10] X. Li, Y. Gao, Y. Yin, L. Wang, and T. Pu, "Experiment and theoretical prediction for surface roughness of PV polycrystalline silicon wafer in electroplated diamond wire sawing," *J. Manuf. Processes*, vol. 49, pp. 82–93, Jan. 2020.
[11] Y. K. Shen, "A novel fabrication method for the mold insert of microlens arrays by hot embossing molding," *Polym. Eng. Sci.*, vol. 46, no. 12, pp. 1797–1803, Dec. 2006.

[12] L. Ma, Y. Gong, and X. Chen, "Study on surface roughness model and surface forming mechanism of ceramics in quick point grinding," *Int. J. Mach. Tools Manuf.*, vol. 77, pp. 82–92, Feb. 2014.
[13] K. Wang, W. C. Sun, F. M. Nie, Q. T. Wu, H. Wu, and S. Li, "Research on the influence of NC quick-point grinding parameters to complex rotator surface roughness," *Appl. Mech. Mater.*, vols. 556–562, pp. 1083–1086, Jan. 2014.
[14] H. Majumder and K. Maity, "Prediction and optimization of surface roughness and micro-hardness using GRNN and MOORA-fuzzy—A MCDM approach for nitinol in WEDM," *Measurement*, vol. 118, pp. 1–13, Mar. 2018.
[15] G. Beruvides, F. Castaño, R. E. Haber, R. Quiza, and A. Villalonga, "A coping with complexity when predicting surface roughness in milling process: Hybrid incremental model with optimal parametrization," *Complexity*, vol. 2017, Dec. 2017, Art. no. 7317254.
[16] G. Beruvides, F. Castaño, R. Quiza, and R. E. Haber, "Surface roughness modeling and optimization of tungsten–copper alloys in micro-milling processes," *Measurement*, vol. 86, pp. 246–252, May 2016.
[17] A. Villalonga, G. Beruvides, F. Castano, and R. E. Haber, "Cloud-based industrial cyber–physical system for data-driven reasoning: A review and use case on an industry 4.0 pilot line," *IEEE Trans. Ind. Informat.*, vol. 16, no. 9, pp. 5975–5984, Sep. 2020.
[18] C. Ahilan, S. Kumanan, N. Sivakumaran, and J. E. R. Dhas, "Modeling and prediction of machining quality in CNC turning process using intelligent hybrid decision making tools," *Appl. Soft Comput.*, vol. 13, no. 3, pp. 1543–1551, Mar. 2013.
[19] N. E. Karkalos and A. P. Markopoulos, "Surface roughness prediction during grinding: A comparison of ANN and RBFNN models," *WSEAS Trans. Syst. Control* vol. 11, pp. 384–390, Jan. 2016.
[20] D. Y. Pimenov, A. Bustillo, and T. Mikolajczyk, "Artificial intelligence for automatic prediction of required surface roughness by monitoring wear on face mill teeth," *J. Intell. Manuf.*, vol. 29, pp. 1045–1061, Jun. 2018.
[21] A. Tharwat and A. E. Hassanien, "Quantum-behaved particle swarm optimization for parameter optimization of support vector machine," *J. Classification*, vol. 36, no. 3, pp. 576–598, Oct. 2019.
[22] D. Kong, Y. Chen, N. Li, C. Duan, L. Lu, and D. Chen, "Tool wear estimation in end milling of titanium alloy using NPE and a novel WOA-SVM model," *IEEE Trans. Instrum. Meas.*, vol. 69, no. 7, pp. 5219–5232, Jul. 2020.
[23] X. Ren, Z. Chai, J. Xu, X. Zhang, Y. He, H. Chen, and X. Chen, "A new method to achieve dynamic heat input monitoring in robotic belt grinding of inconel 718," *J. Manuf. Processes*, vol. 57, pp. 575–588, Sep. 2020.
[24] D. Kong, Y. Chen, N. Li, C. Duan, L. Lu, and D. Chen, "Tool wear estimation in end milling of titanium alloy using NPE and a novel WOA-SVM model," *IEEE Trans. Instrum. Meas.*, vol. 69, no. 7, pp. 5219–5232, Jul. 2020.
[25] W. Huang, H. Liu, Y. Zhang, R. Mi, C. Tong, W. Xiao, and B. Shuai, "Railway dangerous goods transportation system risk identification: Comparisons among SVM, PSO-SVM, GA-SVM and GS-SVM," *Appl. Soft Comput.*, vol. 109, Sep. 2021, Art. no. 107541.
[26] S. Mirjalili and A. Lewis, "The whale optimization algorithm," *Adv. Eng. Softw.*, vol. 95, pp. 51–67, May 2016.
[27] F. Jiang, L. Wang, and L. Bai, "An improved whale algorithm and its application in truss optimization," *J. Bionic Eng.*, vol. 18, no. 3, pp. 721–732, May 2021.